Catalysis Letters Vol. 107, Nos. 3–4, March 2006 (© 2006)
DOI: 10.1007/s10562-005-0007-5

Oxygen-induced restructuring of a Pd/Fe_3O_4 model catalyst

T. Schalow[a], B. Brandt[a], D. E. Starr[a], M. Laurin[a], S. Schauermann[a], Sh. K. Shaikhutdinov[a], J. Libuda[a,b,*], and H. -J. Freund[a]

[a]*Fritz-Haber-Institut der Max-Planck-Gesellschaft, Faradayweg 4-6, D-14195 Berlin, Germany*
[b]*Lehrstuhl für Physikalische Chemie II, Universität Erlangen-Nürnberg, Egerlandstraße 3, D-91058 Erlangen, Germany*

Received 1 November 2005; accepted 16 November 2005

We have studied the influence of oxygen on the structure and morphology of a Pd/Fe_3O_4 model catalyst using molecular beam (MB) methods, IR reflection absorption spectroscopy (IRAS) and scanning tunneling microcopy (STM). The model catalyst was prepared under ultrahigh vacuum (UHV) conditions by physical vapor deposition (PVD) and growth of Pd nanoparticles on an ordered Fe_3O_4 thin film on Pt(111).

It is found that surface oxides are formed on the Pd nanoparticles even under mild oxidation conditions (temperatures of 500 K and effective oxygen partial pressures of around 10^{-6} mbar). These surface oxides are initially generated at the Pd/Fe_3O_4 interface and, subsequently, are formed at the Pd/gas interface. The process of formation and reduction of surface and interface oxides on the Pd particles is fully reversible in that all oxides formed can be fully reduced. As a result, the oxide phase acts like a storage medium for oxygen during oxidation reactions, as probed via CO oxidation.

The process of surface and interface oxidation is directly connected with the onset of a non-reversible sintering process of the Pd particles. It is suggested that this sintering process occurs via a mobile Pd oxide species, which is stabilized by interaction with the Fe_3O_4 support. The restructuring is monitored via STM and IRAS using CO as a probe molecule. In addition to a decrease in particle density and Pd surface area, a reshaping of the particles occurs, which is characterized by the formation of well-ordered crystallites and with a relatively large fraction of (100) facets. After a few oxidation/reduction cycles at 500 K, the sintering process becomes very slow and the system shows a stable behavior under conditions of CO oxidation.

KEY WORDS: palladium; iron-oxide; oxidation; CO; model catalysts; STM; morphology; molecular beams; IR reflection absorption spectroscopy.

1. Introduction

In many cases, the activity of supported metal catalysts critically depends on the size, dispersion and morphology of the active metal particles as well as on the oxide support itself. At the microscopic level, the origin of these effects is poorly understood in many cases. Often it is assumed, that the size and support dependent properties arise from the presence of specific sites at the particle support interface or on the active particles themselves. However, related experimental studies of these properties are seriously complicated by the fact that the active surface may restructure or reconstruct in the presence of reactants. Consequently, microscopic-level models of particle size dependent phenomena including activation and deactivation phenomena require an in depth understanding of the influence of reactants on the catalyst structure.

Oxidation reactions on transition metal surfaces present a particularly intricate situation: numerous studies have reported the formation of different oxide and surface oxide structures, which may be accompanied by significant morphological changes of the surface (see e.g. [1–15] and references therein). In most cases, the mechanisms of oxidation and restructuring are not yet understood, and neither is the effect of the formation of the oxide phases on the activity and selectivity of the catalyst [16–19]. The situation is complicated further for supported metal catalysts, which expose different crystallographic facets, lattice distortions, high defect densities and may show specific interactions at the particle/support interface (compare e.g. [20]). In some cases it has been observed that sintering of the active metal particles may be accelerated at elevated oxygen pressure, which is possibly related to the formation of mobile metal-oxide species facilitating the interparticle transport [21–23], see also [24] and references therein.

Recently, we have demonstrated for a Pd/Fe_3O_4 model catalyst in an oxygen atmosphere that the initial oxidation not only proceeds via the formation of surface oxides at the Pd/gas interface, but instead preferentially occurs at the Pd/support interface [25]. In this study we focus on the effect of surface and interface oxidation on a possible restructuring processes.

In order to obtain detailed structural information on the catalyst surface under reaction conditions, two experimental approaches are combined: First, we employ well-defined oxide-supported model catalysts, which provide clean and well-defined surfaces with strongly reduced complexity. Such model catalysts are

* To whom correspondence should be addressed.
E-mail: libuda@chemie.uni-erlangen.de

easily accessible for various surface science techniques and, therefore, can be characterized in great detail. Specifically, we use Pd nanoparticles deposited by physical vapor deposition (PVD) and growth on a thin and well-ordered Fe_3O_4 film on Pt(111). The model system is prepared *in situ* under ultra-high vacuum (UHV) conditions. Structure, morphology and adsorption properties of the oxide-film [26,27] and the Pd particles [28] have been investigated, previously. Secondly, we have applied a combination of surface science techniques and molecular beam (MB) methods in order to obtain correlated information on surface structure and reactivity. Specifically, we use IR reflection absorption spectroscopy (IRAS) and scanning tunneling microscopy (STM) in combination with MB titration and sticking coefficient measurements.

This approach enables us to study the oxygen uptake and release as well as the kinetics of test reactions under extremely well-defined conditions and, simultaneously, allows us to characterize the particle morphology in detail. Recently, we have shown in a related study that large amounts of oxygen can be reversibly stored and released in form of a thin Pd oxide layer, which is preferentially formed at the particle/support interface [25]. Reduction occurs via release of oxygen from the oxide reservoir onto the metallic part of the surface, where it is readily available for oxidation reactions, such as CO oxidation. In this paper, we show that the oxygen storage process is not only correlated with a reversible formation of surface and interface oxides but also with a non-reversible sintering of the Pd particles. This ripening effect cannot be attributed to pure thermal sintering of the metal particles. Instead, we suggest that the morphological modifications proceeds via the formation of mobile Pd oxide species stabilized by their interaction with the Fe_3O_4 support.

2. Experimental

All molecular beam and IRAS experiments were performed in a UHV apparatus at the Fritz-Haber-Institut (Berlin), which has recently been described in the literature [29]. The system offers the experimental possibility of superimposing up to three molecular beams on the sample surface. A schematic representation of the setup is shown in figure 1. For IRAS experiments, the CO beam (Linde , 99.997%, further purified by a gas filter (Mykrolis)) and O_2 beam (Linde, 99.999%) were generated by doubly differentially pumped effusive sources based on multi-channel arrays. For all experiments presented, the beam intensities were $\sim 2\times10^{14}$ molecules cm^{-2} s^{-1} for CO and O_2 (8×10^{-7} mbar, 0.6 Langmuir/s (1 Langmuir $= 10^{-6}$ Torr s^{-1})). Both sources were operated at room temperature. The beam diameter of the effusive sources was chosen such that it exceeds the sample surface. A CO beam was generated by a triply differentially pumped source from a supersonic expansion and attenuated by means of a mechanical chopper to an intensity of 2.3×10^{13} molecules cm^{-2} s^{-1} (0.05 Langmuir/s). Its diameter was chosen smaller than the sample. For the CO sticking coefficient measurements, which were performed at a sample temperature of 300 K, the non-sticking portion of the incident flux was detected with a non-line-of-sight quadrupole mass spectrometer (ABB Extrel). All IR spectra were acquired using a vacuum FT-IR spectrometer (Bruker IFS 66v) with a spectral resolution of 2 cm^{-1}, and an MIR polarizer to select the p-component of the IR light only.

Scanning Tunneling Microscopy measurements were performed in a separate UHV chamber (at a base pressure of $<2\times10^{-10}$ mbar) equipped with Auger Electron Spectroscopy/Low Energy Electron Diffraction (AES/LEED) (Specs), a Quadrupole Mass Spectrometer (QMS) (Fisons VG) and an STM (Micro H, Omicron) along with standard sample cleaning and preparation facilities. All images were recorded using commercial Pt/Ir tips (LOT-Oriel GmbH) with tunneling currents of approx. 0.7 nA and positive sample biases of approx. 1.4 V.

The thin Fe_3O_4 film ($\sim$100 Å) was grown on Pt(111) by repeated cycles of Fe (>99.99%, Goodfellow) deposition and subsequent oxidation (see [26] for details). Cleanliness and quality of the oxide film was checked by IRAS of adsorbed CO (for MB experiments) and LEED. Pd particles (>99.9%, Goodfellow) were grown by PVD (Pd coverage: 2.7×10^{15} atoms cm^{-2}; sample temperature: 115 K) using a commercial evaporator (Focus, EFM 3, flux calibrated by a quartz microbalance). Directly after Pd deposition, the sample was annealed at 600 K in order to stabilize the Pd particles against thermal sintering.

3. Results and discussion

As a first step to characterize the model system, an STM image of the pristine Pd catalyst was taken

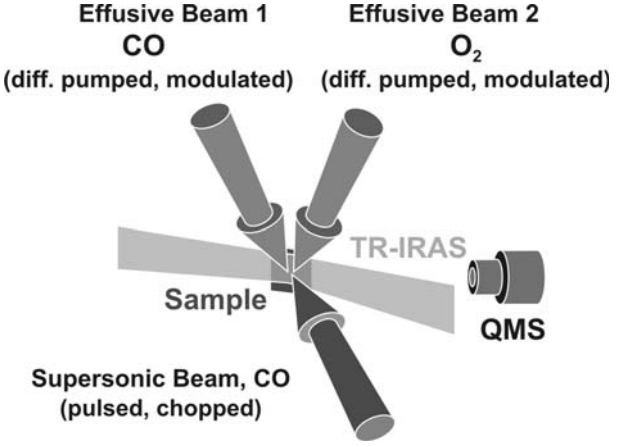

Figure 1. Schematic representation of the molecular beam setup used in this study.

immediately after preparation (figure 2a). The Pd particles have an average diameter of ~4 nm and grow in a (111) orientation with respect to the support. Moreover, the formation of well-defined crystallites uniformly distributed on the iron-oxide surface is observed. The particles predominately expose (111) facets, but also a smaller fraction of (100) facets. Under the growth conditions chosen in this study (2.7×10^{15} Pd atoms cm^{-2}, surface temperature: 115 K, deposition rate: 4.5×10^{12} Pd atoms cm^{-2} s^{-1}), the particle density amounts to 3.8×10^{12} cm^{-2}, corresponding to a Pd dispersion of about 30%. From these numbers, it can be estimated that the particles contain about 700 Pd atoms in average, which is in good agreement with the particle size estimated from STM assuming hemispherical particles.

In figure 2b, an STM image of the same model catalyst after 5 cycles of oxygen exposure (8×10^{-7} mbar for 1000 s, total exposure per cycle: 600 L) and subsequent CO exposure (8×10^{-7} mbar for 3000 s, total exposure per cycle: 1800 L) at 500 K is shown. It becomes immediately evident that the morphology of the catalyst is substantially altered as compared to the pristine system. The island density decreases to about 20% of the original value (8.3×10^{11} islands cm^{-2}), whereas the particle size increases to about 7 nm (3000 atoms). However, the total amount of Pd on the support, which can be estimated from particle size and density, remains unaffected by the oxidation/reduction treatment. For this reason, we can exclude migration of Pd into the iron-oxide support as well as alloying of the Pd particles with iron as possible explanations for the morphological changes. Thus, we rather attribute the particle morphology changes to a pure surface sintering process of the Pd particles arising through an enhanced Pd mobility. It should be noted that the sintering is accompanied by a slight roughening of the iron-oxide support (which immediately after preparation is characterized by atomically flat terraces). STM experiments without Pd on the pure support film show, however, that this roughening is not directly connected to the sintering process, but also occurs on the Pd free support. LEED experiments indicate that the roughening probably occurs as a result of the formation of small Fe_2O_3 islands on the Fe_3O_4 support during oxygen treatment (compare [26]).

It is noteworthy that after few oxidation/reduction cycles at 500 K the sintering process becomes very slow. All kinetic studies are performed on this stabilized surface (typically 5 O_2/CO treatment cycles were used) [25,30]. Only under more drastic conditions can further restructuring occur (at 600 K, the island density decreases to 6.5×10^{11} islands cm^{-2}, corresponding to a Pd particle size of about 8 nm).

In order to investigate how the structural changes affect the adsorption properties of the catalyst, CO sticking coefficient measurements have been performed at 300 K after preparation and after stabilization (5 O_2/CO cycles, see figure 3). Under these conditions, CO adsorbs on the Pd surface only, but not on the iron-oxide support. The sticking coefficient shows a typical precursor-type behavior for both the pristine and the stabilized system, i.e. the sticking probability remains high over a broad coverage range until it drops rapidly when approaching saturation coverage. This behavior is typical for supported metal systems. It arises as a result of classical precursor type adsorption kinetics on the Pd surfaces [31] and a contribution from the so-called "capture-zone" effect (see e.g. [32–34] and references therein). The latter effect involves trapping of CO on the iron-oxide support and subsequent surface diffusion onto the Pd particles. As a result, the sticking probability does not necessarily reflect the surface fraction covered by the Pd particles, but is significantly enhanced. The total CO adsorption capacity amounts to 4.5×10^{14} molecules cm^{-2} for the pristine particles and 3.0×10^{14} molecules cm^{-2} for the stabilized system. When estimating the amount of Pd surface atoms on the basis of the STM data, these values are found to be

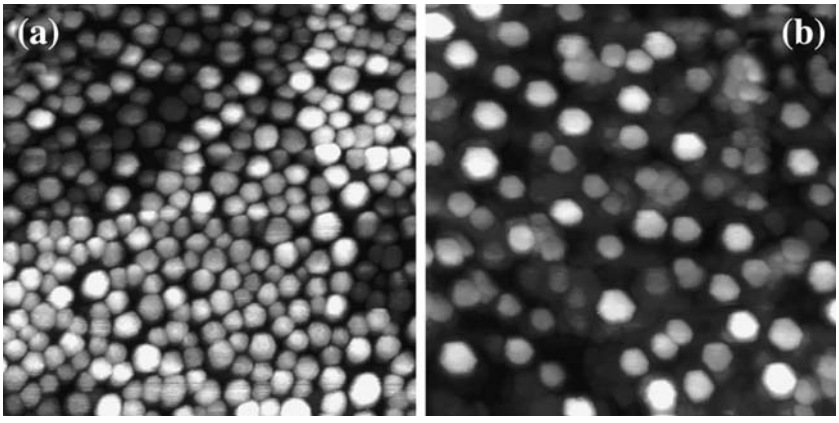

Figure 2. STM images (100×100 nm) of the $Pd/Fe_3O_4/Pt(111)$ model catalyst: (a) after preparation and annealed to 600 K; (b) after five cycles of O_2/CO treatment at 500 K (see text).

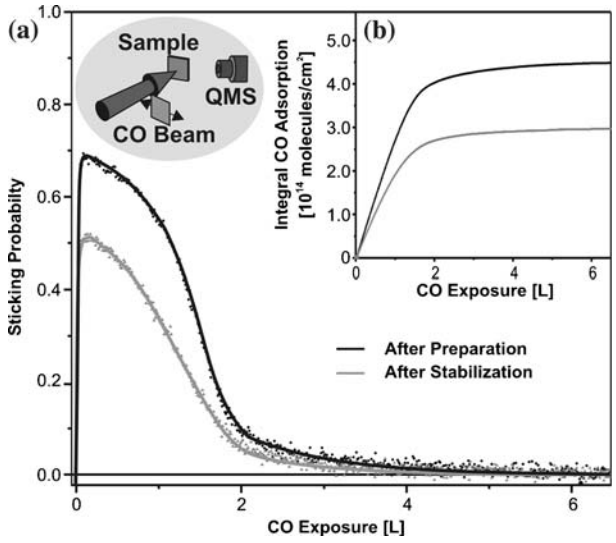

Figure 3. CO sticking coefficient for the $Pd/Fe_3O_4/Pt(111)$ model catalyst at 300 K after preparation and after stabilization with five cycles of O_2/CO treatment at 500 K (see text): (a) CO sticking coefficient; (b) integral CO adsorption.

consistent with a CO saturation coverage of $\theta \sim 0.5$ in both cases (in accordance with the CO saturation coverage on Pd(111) at 300 K [35]).

In order to gain additional information on the mechanism of the sintering process, we perform IR spectroscopy of adsorbed CO after various preparation steps. The use of CO as a probe molecule allows us to monitor morphological changes of the Pd particles in great detail (compare e.g. [36]). In figure 4, IRAS spectra of adsorbed CO at 125 K after different preparation steps are shown. The upper spectrum in figure 4a is taken immediately after preparation of the model catalyst. Here, three different absorption features are observed. Previously, these features have been discussed in detail and assigned in the following manner [37,38]: The feature at a binding energy of 2106 cm^{-1} can be assigned to on-top CO on (111) facets and defect sites, the feature around 1993 cm^{-1} to bridge bonded CO on (100) facets, steps and edge sites and the broad shoulders ranging from 1970 down to 1800 cm^{-1} to CO adsorption mainly on hollow sites on (111) facets. Note that the intensity of the different peaks does not directly reflect the abundance of the corresponding adsorption sites as a result of strong dipole coupling effects (see [39]). Qualitatively, the relative intensities of the different IRAS features are consistent with previous measurements on crystalline Pd particles in the size range of about 1000 atoms [37].

In a first step, an IRAS spectrum of adsorbed CO is taken after annealing the sample in UHV for 3 h at 500 K (see figure 4a). The annealing time in this case is comparable to the total annealing time in the stabilization procedure. Nevertheless, no changes in the spectrum are observed in comparison to the IRAS spectrum taken immediately after preparation. Likewise, STM measurements (not shown) on similar sized particles taken after prolonged (approx.$2\frac{1}{2}$ h.) heating at 500 K, indicated very minor restructuring or sintering of the Pd particles.

In a next step the influence of oxygen is investigated by performing oxidation/reduction cycles (600 L O_2, 1800 L CO) at different sample temperature (see figure 4a and b)). After treatment at 400 K no changes in the CO IRAS spectra can be detected, as well as no restructuring or sintering observed in the STM images. However, on treatment at 500 K and above, the CO IRAS spectra are subject to significant changes. The CO absorption feature at 1993 cm^{-1} shows a blue-shift to

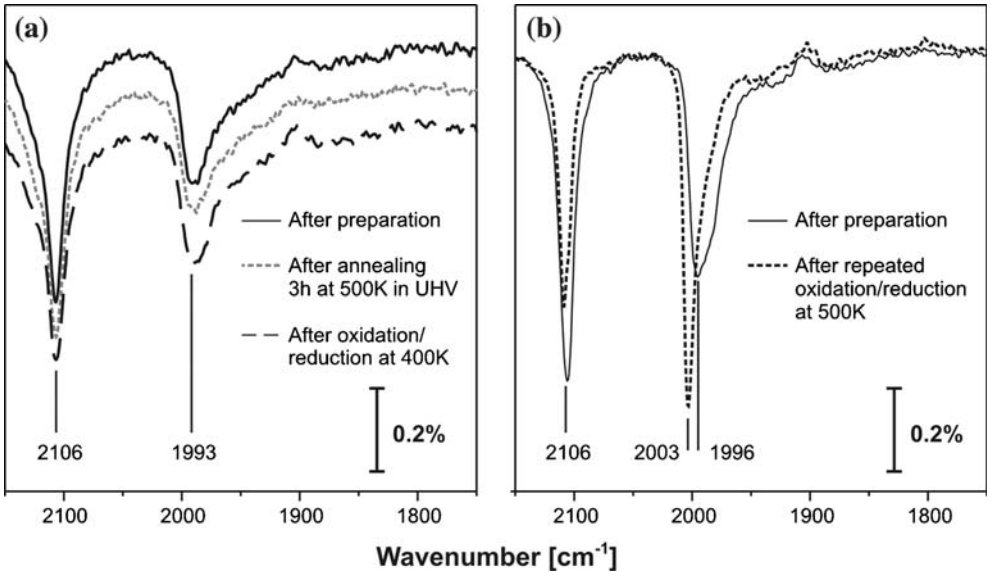

Figure 4. IR reflection absorption spectra of the CO stretching frequency region for CO adsorption at 125 K on the $Pd/Fe_3O_4/Pt(111)$ model catalyst.

2000 cm^{-1} and gains intensity at the expense of the on-top feature at 2106 cm^{-1}. Additionally, both peaks become significantly sharper as compared to the pristine sample.

In single crystal studies on Pd(111) it has previously been shown that up to 400 K oxygen adsorbs dissociatively, forming a p(2×2) structure of chemisorbed atomic oxygen (see e.g. [40]). This process is not accompanied by reconstructions of the Pd surface. Similarly, oxygen forms chemisorbed overlayers of atomic oxygen at 400 K on supported Pd particles [25]. For oxidation temperatures of 500 K and above, however, we have recently shown that a thin interface oxide layer is generated, followed by the formation of surface oxides at the Pd/vacuum interface [25]. The formation of Pd surface oxides has also been reported on single crystal surfaces (see e.g. [11,12] and references therein). However, the above work [25] suggests that on single crystal surfaces these oxide layers are thermodynamically less stable than on the dispersed particle systems and that their formation is also subject to stronger kinetic hindrances. It is noteworthy that the formation of surface and interface oxide layers is associated with a strong restructuring of the Pd surface layer and thus implies significant mobility of the Pd containing species.

From theses results, it can be concluded that a pure physical ripening process, based on the dissociation of Pd atoms from the particles and diffusion on the support can be excluded. Obviously, the presence of oxygen, even if the partial pressure is low, represents a crucial prerequisite for sintering in the present study. Moreover, the onset of sintering (500 K) coincides with the onset of formation of the interface oxide layer. No sintering is observed at conditions at which only surface chemisorption occurs, i.e. at 400 K. On the other hand it is found that neither full surface oxidation nor bulk oxidation of the Pd particles is required in order to facilitate the sintering process. Hence, we assume that sintering occurs via a ripening mechanism directly associated with the formation of the Pd interface oxide layer. We suggest that, in connection with the oxidation and restructuring of the Pd/support interface, mobile Pd_xO_y species are generated, which may be stabilized by the support. The sintering process should then involve mass transport between Pd particles via these mobile Pd oxide species.

In order to further substantiate this hypothesis, the formation of Pd surface and interface oxides was studied by IRAS. In these experiments, the stabilized catalyst was exposed to O_2 at different temperatures. Following this treatment, the sample was cooled to 250 K in O_2, leading to formation of a saturated chemisorbed oxygen layer on the metallic Pd surface (e.g. a p(2×2) structure for Pd(111) [1]). After cooling the sample in UHV to 125 K, CO was coadsorbed. Finally, IRAS spectra of the CO stretching frequency region were taken (see top schematic in figure 5). Based on single crystal experiments, the formation of O + CO phases are expected under these conditions (e.g. a mixed $p(2\times2)_{O+CO}$ phase on Pd(111) [41]). In figure 5, the corresponding IRAS spectra after oxidation at different temperatures are shown. The spectra of the coadsorption phase consist of one peak at 2133 cm^{-1} and a broad feature centered at approx. 1950 cm^{-1}, which is in agreement with previous studies (see [42]). It is observed that for oxidation temperatures higher than 500 K, the intensity of both IRAS features decreases until it almost vanishes for oxidation at 600 K.

We attribute the decrease in intensity of the IRAS features to the formation of surface oxides on the Pd particles, leading to a decrease of the metallic Pd surface area available for CO adsorption. Since no features typical for CO adsorption on oxides appear in the IRAS spectrum after oxidation at 600 K, we concluded that CO does not adsorb on the Pd surface oxides under the conditions applied.

The inset in figure 5 shows the relative integral intensities of adsorbed CO in the IRAS spectra after oxidation at different temperatures (normalized to the spectra taken after oxygen exposure at 300 K, i.e. oxygen chemisorption without formation of surface oxides). For oxidation temperatures up to 475 K almost no changes in the intensities of the IRAS spectra are observed indicating pure chemisorption only. For oxidation temperatures of 500 K and above, the intensity of the IRAS features for adsorbed CO decrease, indicating the formation of Pd surface oxides. The onset temperature for the formation of these surface oxides is approximately 500 K for the oxygen partial pressure and oxidation times applied in this work. Again, it should be noted that the IRAS intensities do not yield accurate quantitative information on the surface coverage. Still it is apparent that in the temperature range between 500 and 600 K metallic and oxidized areas coexist on the Pd particles. In the previous study it was shown that at 500 K an interface oxide at the Pd/Fe_3O_4 is formed, without major changes of the outer surface of the Pd particles [25]. This finding is consistent with the minor changes observed for the CO IR spectra at this temperature. At higher temperatures, the Pd/vacuum interface becomes oxidized also. Finally at 600 K, almost the entire surface of the Pd particle is covered by surface oxides. It is important to point out that the formation of surface and interface oxides is fully reversible. Upon CO exposure at 500 K fully metallic Pd surface can be reestablished [25].

The main conclusion from this experiment is that indeed the onset of the sintering process coincides with the temperature limit for the formation of the interface oxide. These findings provide further evidence for our hypothesis that the sintering process is coupled to the formation of Pd oxides species, in particular to the formation of the Pd/Fe_3O_4 interface oxide. Via transient molecular beam experiments we have recently investi-

gated the formation of the interface oxide and have shown that it is significantly stabilized by the Fe_3O_4 support [25,30]. It might be expected that these strong interactions between Pd interface oxide species and the oxide support may also stabilize a mobile Pd oxide species, which facilitates the ripening process. Consequently it should be expected that as a result of this mechanism the stability of the mobile Pd oxide species and, therefore, the temperature onset for sintering should strongly depend on the type and surface properties of the support.

Finally, it is noteworthy to briefly consider the morphology of the Pd particles on the Fe_3O_4 support. A comparison with previous studies of the Pd growth on an ordered alumina support (Al_2O_3/NiAl(110)) is shown in figure 6 [38,43]. On Fe_3O_4, Pd grows in (111) orientation and initially forms hexagonally shaped particles of about 4 nm diameter, which are terminated by a large (111) terrace on top and (111) as well as (100) facets at the particle sides. After oxygen induced sintering, the average particle size increases to about 7 nm diameter (3000 Pd atoms). This process is accompanied by the formation of larger and well-ordered facets, as reflected in both the STM images and the IRAS data. For the preparation conditions used here, the (111) top facets account for ~40%, the side (111) facets for ~30% and the (100) side facets for ~30% of the total Pd surface.

For Pd grown on Al_2O_3, similar particles sizes as for the Pd/ Fe_3O_4 system are observed under appropriate preparation conditions [43]. Under the conditions used for preparation of the sample shown in figure 6 (right column), the particles have a diameter of about 6 nm. Another similarity between both system is the (111) orientation and the termination by a large (111) top facet as well as (111) and (100) side facets. The ratio of (111) and (100) side facets differs, however, for both systems. For the Pd/Al_2O_3 the fraction of the (100) facets is significantly smaller and typically accounts for less than 20% of the total Pd surface. It is anticipated that an increased interaction with support for the Pd/ Fe_3O_4 system in comparison with the Pd/Al_2O_3 may be responsible for this difference in particle shape.

In figure 6 a direct comparison of the CO IR spectra is displayed, demonstrating that these morphological changes can directly be monitored via IRAS of the CO stretching frequency region (it should be noted that the spectra strongly depend on coverage and, therefore, this type of comparison requires very similar experimental conditions in all cases): for the small Pd particles on Fe_3O_4 before sintering, CO adsorption is dominated by on-top species and bridge bonded CO, mainly at particle edge and defect sites (see e.g. [38,44] and references therein). The two species give rise to the intense on-top peak (2106 cm^{-1}) and the broader feature at

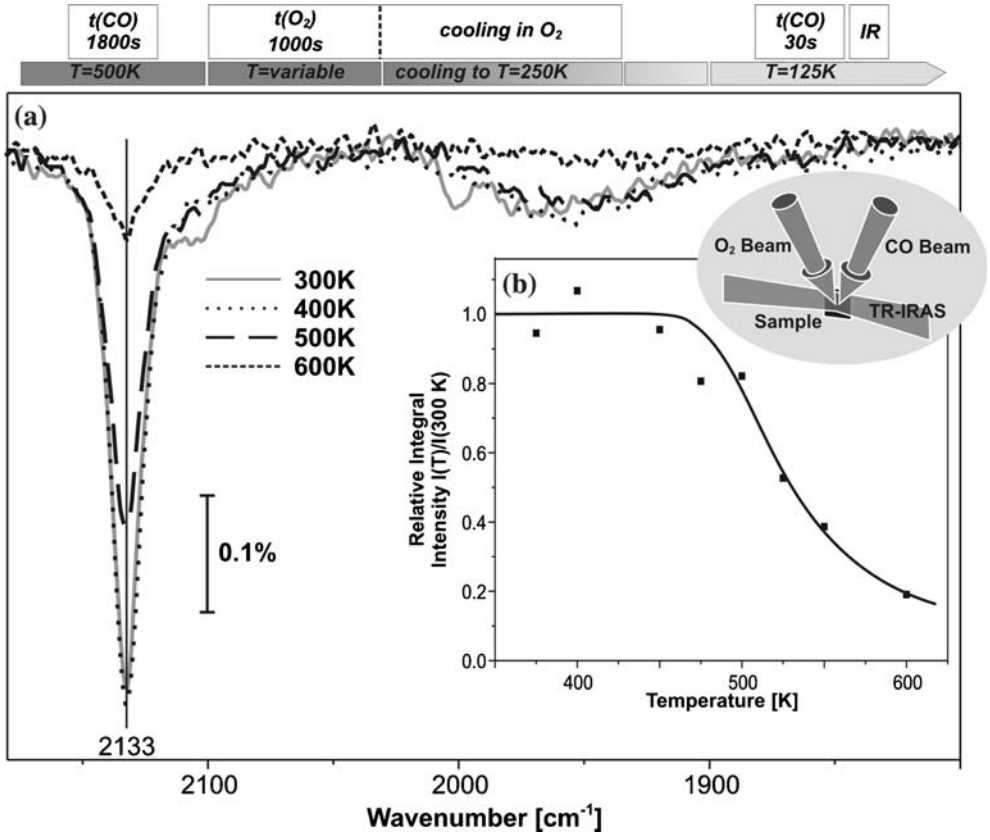

Figure 5. IR reflection absorption spectra of the CO stretching frequency region for co-adsorption of CO and O on $Pd/Fe_3O_4/Pt(111)$ at 125 K for various oxidation temperatures. Inset: integral CO absorption signal as a function of oxidation temperature after saturation of the remaining metallic part of the Pd surface by CO, O co-adsorption layer.

(1996 cm^{-1}). Strong intensity transfer from the lower frequency range (below 1990 cm^{-1}) to the latter feature decreases the spectral intensity at lower wavenumber (which is mainly due to CO on hollow sites). After oxygen induced sintering the decreasing defect density and increasing facet size leads to a decreasing abundance of on-top CO. Both the increasing facet size and the increasing fraction of (100) facets give rise to a sharpening and blue-shift of the CO bridge band to around 2003 cm^{-1}. For the Pd particles on Al_2O_3, the fraction of (100) facets is smaller. This leads to a broader CO bridge band, which is now dominated by CO adsorbed at particle edges and defects. We conclude that the CO IR spectra are in good agreement with the STM results and can indeed be utilized as a very sensitive structural probe for monitoring changes of the average Pd particle shape.

4. Conclusions

We have studied the sintering mechanism for oxide supported Pd nanoparticles. Combining molecular beam methods, various surface science techniques and well-defined model catalysts, we have investigated morphological changes of the catalyst surface upon thermal treatment in UHV and under the influence of oxygen. Two effects are observed:

i. *Reversible surface and interface oxidation*: For oxidation temperatures of 500 K and above at effective oxygen pressures of around 10^{-6} mbar thin Pd oxide layers are formed on the Pd particles. Initial oxidation at 500 K occurs at the Pd/Fe_3O_4 interface. At sample temperatures above 500 K, a part of the Pd/gas interface is also oxidized. Its fraction increases with increasing temperature. In the temperature range between 500 and 600 K, metallic Pd and Pd surface/interface oxides are found to co-exist on the particles. The formation of the surface and interface oxides is fully reversible. The catalyst can be completely reduced by CO exposure ($\sim 10^{-6}$ mbar) at 500 K.

ii. *Non-reversible oxygen-induced sintering of Pd particles*: The formation of Pd interface oxide species is directly associated with the onset of a non-reversible sintering of the Pd particles. Similar sintering processes do not occur under UHV conditions at the same temperatures. It is suggested that the ripening

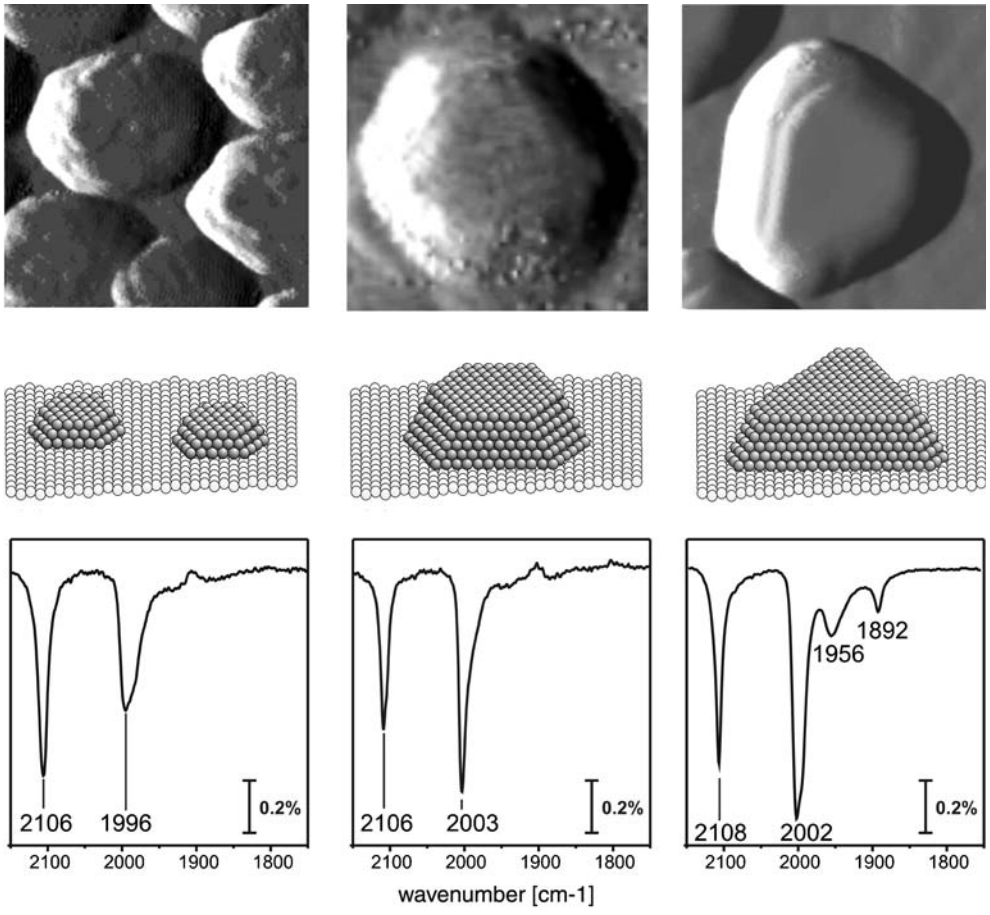

Figure 6. STM close-up images (12×12 nm), schematic representations of the particles and IRAS spectra of CO adsorbed at 125 K on the Pd particles: (left) $Pd/Fe_3O_4/Pt(111)$ model catalyst after preparation; (middle) $Pd/Fe_3O_4/Pt(111)$ model catalyst after repeated O_2/CO treatment at 500 K; (right) $Pd/Al_2O_3/NiAl(110)$ model catalyst (STM and IRAS spectrum of Pd/Al_2O_3 by M. Frank and M. Bäumer [38]).

process occurs via the formation of a mobile Pd oxide species, which is stabilized by interaction with the Fe_3O_4 support.

Changes in particle size, density and shape were monitored by a combination of STM and IRAS using CO as a probe molecule. Detailed information on the particle shape is available from an analysis of the CO stretching frequency region. It was found that the oxygen-induced sintering process leads to the formation of well shaped Pd crystallites, which grow in (111) orientation on the Fe_3O_4 film. In addition to a majority of (111) facets, these crystallites are terminated by a relatively large fraction of (100) facets.

Acknowledgements

This work has been funded by the Deutsche Forschungsgemeinschaft (SPP 1091) and the Fonds der Chemischen Industrie. The authors are particularly grateful to M. Bäumer for providing STM images and IRAS spectra of Pd on Al_2O_3.

References

[1] H. Conrad, G. Ertl, J. Küppers and E.E. Latta, Surf. Sci. 65 (1977) 235.
[2] R. Imbihl and J.E. Demuth, Surf. Sci. 173 (1986) 395.
[3] T.W. Orent and S.D. Bader, Surf. Sci. 176 (1986) 395.
[4] S.-L. Chang and P.A. Thiel, J. Chem. Phys. 88 (1988) 2071.
[5] V.A. Bondzie, P. Kleban and D.J. Dwyer, Surf. Sci. 347 (1996) 319.
[6] E.H. Voogt, A.J.M. Mens and J.W.G.O.L.J. Gijzeman, Surf. Sci. 373 (1997) 210.
[7] F.P. Leisenberger, G. Koller, M. Sock, S. Surnev, M.G. Ramsey, F.P. Netzer, B. Klötzer and K. Hayek, Surf. Sci. 445 (2000) 380.
[8] V.A. Bondzie, P.H. Kleban and D.J. Dwyer, Surf. Sci. 465 (2000) 266.
[9] G. Zheng and E.I. Altman, Surf. Sci. 462 (2000) 151.
[10] G. Zheng and E.I. Altman, Surf. Sci. 504 (2002) 253.
[11] E. Lundgren, G. Kresse, C. Klein, M. Borg, J.N. Andersen, M. De Santis, Y. Gauthier, C. Konvicka, M. Schmid and P. Varga, Phys. Rev. Lett. 88 (2002) 246103.
[12] M. Todorova, E. Lundgren, V. Blum, A. Mikkelsen, S. Gray, J. Gustafson, M. Borg, J. Rogal, K. Reuter, J.N. Andersen and M. Scheffler, Surf. Sci. 541 (2003) 101.
[13] E. Lundgren, J. Gustafson, A. Mikkelsen, J.N. Andersen, A. Stierle, H. Dosch, M. Todorova, J. Rogal, K. Reuter and M. Scheffler, Phys. Rev. Lett. 92 (2004) 046101.
[14] M. Todorova, K. Reuter and M. Scheffler, Phys. Rev. B 71 (2005) 195403.
[15] H. Over, Y.D. Kim, A.P. Seitsonen, S. Wendt, E. Lundgren, M. Schmid, P. Varga, A. Morgante and G. Ertl, Science 287 (2000) 1474.
[16] M.R. Basset and R. Imbihl, J. Chem. Phys. 93 (1990) 811.
[17] G. Zheng and E.I. Altmann, J. Phys. Chem. B 2002 (2002) 1048.
[18] E.I. Altman, 2003, 547, 108.
[19] B.L.M. Hendriksen, S.C. Bobaru and J.W.M. Frenken, Surf. Sci. 552 (2004) 229.
[20] H. Graoui, S. Giorgio and C.R. Henry, Surf. Sci. 417 (1998) 350.
[21] P. Wynblatt and N.A. Gjostein, in: *Progress in Solid State Chemistry,* Vol. 9, eds. J.O. McCaldin and G.A. Somorjai, (1975), 21 pp.
[22] X. Lai and D.W. Goodman, J. Mol. Catal. A 162 (2000) 33.
[23] C.H. Bartholomew, in: *Catalyst Deactivation*, C.H. Bartholomew and G.A. Fuentes (eds), (Elsevier, 1997), 585 pp.
[24] C.T. Campbell, S.C. Parker and D.E. Starr, Science 298 (2002) 811.
[25] T. Schalow, B. Brandt, M. Laurin, S. Guimond, D.E. Starr, H. Kuhlenbeck, S.K. Shaikhutdinov, J. Libuda and H.-J. Freund, Angew. Chem. Int. Ed. (in press).
[26] W. Weiss and W. Ranke, Prog. Surf. Sci. 70 (2002) 1.
[27] C. Lemire, R. Meyer, V. Henrich, S.K. Shaikhutdinov and H.-J. Freund, Surf. Sci. 572 (2004) 103.
[28] R. Meyer, S.K. Shaikhutdinov and H.-J. Freund, Z. Phys. Chem. 218 (2004) 2004.
[29] J. Libuda, I. Meusel, J. Hartmann and H.-J. Freund, Rev. Sci. Instrum. 71 (2000) 4395.
[30] T. Schalow, B. Brandt, M. Laurin, J. Libuda and H.-J. Freund (in preparation).
[31] T. Engel, J. Chem. Phys 69 (1978) 373.
[32] C.R. Henry, Surf. Sci. Rep. 31 (1998) 231.
[33] V.P. Zhdanov and B. Kasemo, Surf. Sci. Rep 39 (2000) 25.
[34] J. Libuda and H.-J. Freund, Surf. Sci. Rep. 57 (2005) 157.
[35] A.M. Bradshaw and F.M. Hoffman, Surf. Sci. 72 (1978) 513.
[36] S. Bertarione, D. Scarano, A. Zecchina, V. Johanek, J. Hoffmann, S. Schauermann, M.M. Frank, J. Libuda, G. Rupprechter and H.-J. Freund, J. Phys. Chem. B 108 (2004) 3603.
[37] K. Wolter, O. Seiferth, H. Kuhlenbeck, M. Bäumer and H.-J. Freund, Surf. Sci. 399 (1998) 190.
[38] M. Frank and M. Bäumer, Phys. Chem. Chem. Phys. 2 (2000) 3723.
[39] P. Hollins, Surf. Sci. Rep. 16 (1992) 51.
[40] H. Conrad, G. Ertl, J. Küppers and E.E. Latta, Surf. Sci. 65 (1977) 245.
[41] J. Mendez, S.H. Kim, J. Cerda, J. Wintterlin and G. Ertl, Phys. Rev. B 71 (2005) 085409.
[42] X. Xu and D.W. Goodman, J. Phys. Chem. 97 (1993) 7711.
[43] I. Meusel, J. Hoffmann, J. Hartmann, M. Heemeier, M. Bäumer, J. Libuda and H.-J. Freund, Catal. Lett. 71 (2001) 5.
[44] I.V. Yudanov, R. Sahnoun, K.M. Neyman, N. Rösch, J. Hoffmann, S. Schauermann, V. Johánek, H. Unterhalt, G. Rupprechter, J. Libuda and H.-J. Freund, J. Phys. Chem. B 107 (2003) 255.